J Math Chem (2009) 45:95–112
DOI 10.1007/s10910-008-9370-y

ORIGINAL PAPER

Formation and control of Turing patterns and phase fronts in photonics and chemistry

Gian-Luca Oppo

Received: 13 June 2007 / Accepted: 21 November 2007 / Published online: 6 May 2008

Abstract We review the main mechanisms for the formation of regular spatial structures (Turing patterns) and phase fronts in photonics and chemistry driven by either diffraction or diffusion. We first demonstrate that the so-called 'off-resonance' mechanism leading to regular patterns in photonics *is* a Turing instability. We then show that negative feedback techniques for the *control* of photonic patterns based on Fourier transforms can be extended and applied to chemical experiments. The dynamics of phase fronts leading to locked lines and spots are also presented to outline analogies and differences in the study of complex systems in these two scientific disciplines.

Keywords Photonics · Chemistry · Turing patterns · Control · Phase fronts · Localized states · Spots

1 Introduction

Since the pioneering work of Alan Turing on chemical morphogenesis [1], it has become clear that two species diffusing at different rates and competing with each other within the same environment can spontaneously break the translational invariance (discretely) leading to the formation of regular (and irregular) spatial patterns. Although the Turing instability can be studied in linearized systems (see [2] and Sect. 2), nonlinearity is necessary to saturate the growth of the unstable mode of the pattern. Above the Turing instability a variety of geometrical structures (stripes, squares, rhomboids, hexagons, honeycombs, etc.) can form in a 2D space, their relative stability depending on the details of the given equations and nonlinear terms. The simultaneous presence

G.-L. Oppo (✉)
SUPA and Department of Physics, Institute of Complex Systems at Strathclyde,
University of Strathclyde, 107 Rottenrow, Glasgow G4 ONG, UK
e-mail: gianluca@phys.strath.ac.uk

of several steady states is an intrinsic evidence of nonlinearity. Here we present the formation and control of regular (the spatially periodic patterns mentioned above), irregular and localized spatio-temporal structures in photonic and chemical systems and discuss analogies and differences between these two scientific disciplines.

The paper is organized as follows. In Sect. 2 we review Turing instabilities leading to pattern formation in the presence of diffusion (diffraction), the main mechanism for spatial coupling in chemistry (photonics). We demonstrate, in Sect. 3, that the so-called "off-resonance" mechanism typical of the formation of patterns in certain photonic systems driven by diffraction *is* a Turing process; there is a single universality class that encompasses reaction–diffusion and off-resonance instabilities leading to Turing patterns in chemistry and photonics. Negative feedback techniques based on Fourier filtering and used to control regular and turbulent spatial structures are reviewed in Sect. 4. A great deal of theoretical and experimental techniques developed in photonics [3] can be applied and profitably exported to control Turing patterns in chemical systems. Section 5 is instead devoted to the formation and motion of phase fronts in systems that appear in chemistry and photonics and that are characterized by a nonconserved order parameter. In particular we discuss the locking mechanism of phase fronts that leads to stable lines and spots in 2D. Conclusions and the prospective of a closer collaboration between chemists and photonic physicists in the area of spatio-temporal structures are presented in Sect. 6.

2 Turing instabilities and pattern formation in chemistry

In his seminal paper on chemical morphogenesis in 1952, Alan Turing showed that the translational invariance of a homogenous solution can spontaneously break in systems with competing species (an activator and an inhibitor) with separate diffusion rates [1]. An excellent review and expansion of Turing's work is provided in [4]. Here we use a simplified 'linearized' model of the Turing instability in 1D as discussed in [2]:

$$\begin{aligned} \partial_t \mathrm{R} &= \alpha \mathrm{R} - \beta \mathrm{I} + \mathrm{D}_1 \partial_x^2 \mathrm{R} \\ \partial_t \mathrm{I} &= \gamma \mathrm{R} - \delta \mathrm{I} + \mathrm{D}_2 \partial_x^2 \mathrm{I} \end{aligned} \tag{2.1}$$

where the parameters $\alpha, \beta, \gamma, \delta$ and the diffusion rates D_1 and D_2 are real and positive quantities. Since R (I) displays linear growth (decay), it is identified as the activator (inhibitor) variable of the two diffusing species. The homogeneous solution $\mathrm{R}=\mathrm{I}=0$ is unstable to a spatially modulated perturbation of wave-vector $\mathrm{k_c} = 2\pi/\Lambda_\mathrm{c}$ with

$$\mathrm{k_c^2} = \left(\frac{2\pi}{\Lambda_\mathrm{c}}\right)^2 = \frac{1}{2}\left[\frac{\alpha}{\mathrm{D}_1} - \frac{\delta}{\mathrm{D}_2}\right] \tag{2.2}$$

if and only if

$$\frac{\mathrm{D}_2}{\mathrm{D}_1} > \frac{\delta}{\alpha}. \tag{2.3}$$

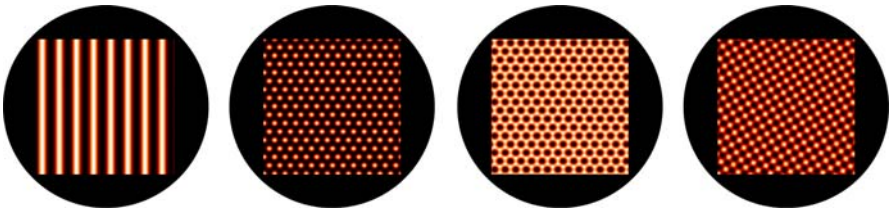

Fig. 1 Possible patterns above the Turing instability: stripes, hexagons, honeycombs and squares

Since there are no nonlinear terms in Eq. 2.1, the amplitude of the Turing pattern (i.e. a spatially periodic solution with wavelength Λ_c) grows indefinitely. The main role of the nonlinear terms is in fact to counterbalance such linear growth via saturation (see [2,4]). In 2D the Turing instability does not prescribe a given geometry provided that the spatial periodicity is $\Lambda_c = 2\pi/k_c$. Several geometries can tile the 2D plane: stripes, squares, rhomboids, hexagons, honeycombs, etc. (see Fig. 1).

The saturating nonlinear terms do not affect the simultaneous existence of the separate geometries but only their relative stability. We will see in Sect. 4 how this fact can be used to our advantage in devising effective and experimentally feasible control methods for pattern formation. We can now summarize the necessary features of an instability leading to Turing patterns as follows [4]:

(a) a clear activator-inhibitor linear dynamics and
(b) specific conditions on the spatial coupling mechanism allowing or forbidding pattern formation.

Clear-cut experimental demonstrations of the formation of stationary Turing patterns in chemical reactions have been realized in the early nineties in Bordeaux (France) by the group of de Kepper [5] and in Austin (TX, USA) by the group of Swinney [6] using a Chlorite and Iodide reaction with Malonic Acid (CIMA). Transitions from the homogeneous to either a hexagonal or a striped structure have been observed when decreasing the temperature (see Fig. 2). Turing instabilities in other chemical systems,

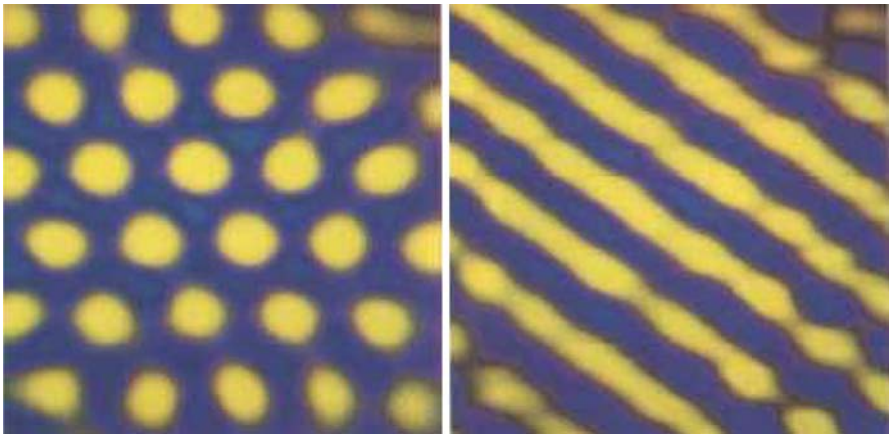

Fig. 2 Turing patterns in the CIMA reaction obtained from a homogeneous state upon decreasing the temperature [6]. Hexagons are observed first and then stripes. Courtesy of H.L. Swinney

such as, for example, the Ostwald ripening [7], have also been demonstrated, with experimental evidence dating to as early as 1973 [8]. Turing patterns in the Belosuov-Zhabotinsky (BZ) reaction, the prototype of reaction–diffusion systems in chemistry, have also been observed in a water-in-oil aerosol OT micro-emulsion (BZ-AOT) [9]. A detailed history of Turing instabilities and structures in chemistry is however beyond the scope of this paper.

3 Turing instabilities and pattern formation in photonics

The main mechanism of spatial coupling for pattern formation in photonic systems is diffraction and not diffusion. To understand the origin and the mathematical treatment of diffraction, we consider the Maxwell equations for the propagation of light (electromagnetic waves) in a nonmagnetic medium with no free currents:

$$\nabla \times \tilde{\mathbf{E}} = -\frac{\partial \tilde{\mathbf{B}}}{\partial \mathrm{t}} \quad \nabla \times \tilde{\mathbf{B}} = \frac{1}{\mu_0}\frac{\partial \tilde{\mathbf{D}}}{\partial \mathrm{t}}$$
$$\nabla \cdot \tilde{\mathbf{D}} = 0 \quad \nabla \cdot \tilde{\mathbf{B}} = 0 \quad \tilde{\mathbf{D}} = \varepsilon_0 \tilde{\mathbf{E}} + \tilde{\mathbf{P}} \tag{3.1}$$

where $\tilde{\mathbf{E}}$, $\tilde{\mathbf{B}}$, $\tilde{\mathbf{D}}$, $\tilde{\mathbf{P}}$ are the (real) electric, magnetic, material and displacement (or polarization) fields, ε_0 and μ_0 are the electrical permittivity and the magnetic permeability, respectively, and such that $\mathrm{c} = (\varepsilon_0\mu_0)^{-1/2}$ is the speed of light in a vacuum. All responses and properties of the material are contained within the polarization field. If we want to merge Maxwell's equations into a single partial differential equation it is useful to take the curl of the curl of the electric field vector and to use the vector calculus equality

$$\nabla \times (\nabla \times \tilde{\mathbf{E}}) = \nabla(\nabla \cdot \tilde{\mathbf{E}}) - \nabla^2 \tilde{\mathbf{E}}, \tag{3.2}$$

where the first term on the l.h.s is the gradient of the divergence of the electric field, while the second is the Laplacian operator in 3D. The latter is due to diffraction and describes the fact that each point on the wave front of an electromagnetic wave becomes a source of a 3D spherical wave. Diffraction was first studied theoretically by C. Huygens and later by A. Fresnel and J. Fraunhofer.

One can now take advantage of the strong directionality of laser beams used in modern photonic devices and rewrite the electric and polarization fields as slowly varying (in t and z) complex amplitudes multiplied by carriers at the optical frequency ω_0 and wave-vector $\mathrm{k_z}$:

$$\tilde{\mathbf{E}} = \mathbf{E}(\mathrm{t,x,y})\ \exp[\mathrm{i}(\mathrm{k_z z} - \omega_0 \mathrm{t})] + \text{complex conjugate}$$
$$\tilde{\mathbf{P}} = \mathbf{P}(\mathrm{t,x,y})\ \exp[\mathrm{i}(\mathrm{k_z z} - \omega_0 \mathrm{t})] + \text{complex conjugate}$$

where x and y are the so-called 'transverse' coordinates since they are perpendicular to the direction of the propagation of light z. By considering a single direction of polarization (i.e. linearly polarized light) the vector notation may be dropped and,

using the paraxial and the slowly varying approximations, a single Maxwell equation can be obtained:

$$\partial_\tau \mathrm{E} = \mathrm{ia}\ (\mu_0\omega_0^2\mathrm{P} + \nabla^2\mathrm{E}) = \mathrm{ia}\mu_0\omega_0^2\mathrm{P} + \mathrm{ia}(\partial_\mathrm{x}^2 + \partial_\mathrm{y}^2)\mathrm{E} \tag{3.3}$$

where i is the square root of -1, $\mathrm{a} = \mathrm{c}/(2\mathrm{k_z})$ and $\tau = \mathrm{z} - \mathrm{ct}$. This equation (or several of them in the case of interacting fields of different frequencies) is, in general, coupled to differential equations that describe the polarization field inside the material and provided with boundary and propagation conditions that describe optical elements such as mirrors, waveguides, apertures, dispersion compensators, etc.

Further approximations are feasible (see in particular the mean field limit for cavity-based photonic devices) but the structure of Eq. 3.3 with respect to diffraction (the Laplacian) remains unchanged. We note here that the main differences with respect to reaction–diffusion systems such as the Turing model of Sect. 2, are that the field amplitude E is complex and the diffractive spatial coupling is multiplied by the imaginary number i. The relevance of these considerations will be seen later when demonstrating that 'off-resonance' photonic patterns are Turing structures.

Early links between Turing and optical patterns were made in a seminal paper by Lugiato and Lefever [10]. A clear activator-inhibitor dynamics, however, was not established. We now show that the latter is possible for photonic systems displaying the so called 'off-resonance' mechanism for the formation of stationary patterns. 'Off-resonance' pattern formation corresponds to the generation of periodic spatial structures whose spatial modulation is inversely proportional to the square root of the detuning between the material and cavity resonances. As an example of a photonic device that displays 'off-resonance' pattern formation, we consider the Degenerate Optical Parametric Oscillator (DOPO) [11] in the specific configuration of a nonresonated pump field. We consider one spatial transverse dimension for simplicity and for an effective comparison with the models of Sect. 2. The results, however, do not change in the 2D case of a transverse plane (x,y). The final equation for the signal field E has the form of a Parametrically Forced Ginzburg-Landau (PFGL) equation [12]:

$$\partial_\tau \mathrm{E} = \mathrm{Q}\,\mathrm{E}^* - (1 + \mathrm{i}\Delta)\mathrm{E} - \mathrm{E}|\mathrm{E}|^2 + \mathrm{ia}\ \partial_\mathrm{x}^2\mathrm{E}, \tag{3.4}$$

where * represents the complex conjugate operation, Q is the real amplitude of the input pump and Δ is the detuning between the signal frequency and the closest cavity mode. By introducing the real (R) and imaginary (I) part of the signal field E, Eq. 3.4 becomes

$$\begin{aligned} \partial_\mathrm{t}\mathrm{R} &= (\mathrm{Q} - 1)\mathrm{R} + \Delta\mathrm{I} - \mathrm{a}\ \partial_\mathrm{x}^2\mathrm{I} - \mathrm{R}(\mathrm{R}^2 + \mathrm{I}^2) \\ \partial_\mathrm{t}\mathrm{I} &= -\Delta\mathrm{R} - (1 + \mathrm{Q})\mathrm{I} + \mathrm{a}\ \partial_\mathrm{x}^2\mathrm{R} - \mathrm{I}(\mathrm{R}^2 + \mathrm{I}^2). \end{aligned} \tag{3.5}$$

The nonlinear terms have a purely saturating role for both variables R and I. In order to characterize the linear onset of the instability, we neglect them ($|\mathrm{R}|, |\mathrm{I}| << 1$). When setting the diffraction coefficient to zero (a=0), the linear term structure of Eq. 3.5 exactly reproduces that of Eq. 2.1 with zero diffusion rates, under the identification of $\alpha = \mathrm{Q} - 1$, $\beta = \gamma = -\Delta$, $\delta = \mathrm{Q} + 1$. In the DOPO system, then, the real

(imaginary) part of the complex electric field plays the role of the activator (inhibitor). This is condition (a) of the Turing instability as established in Sec. 2. It is no surprise that a second photonic system considered here in Sect. 4 (see Eq. 4.3 for a saturable absorber) and capable of producing Turing structures, leads to exactly the same set of linearized equations for an activator and inhibitor dynamics. Note that diffraction exchanges the spatial derivatives between the activator and inhibitor. Since we want to find out if DOPO spatial periodic structures belong to the same class of universality of Turing patterns, we study Eq. 3.5 with no nonlinear terms and with generic diffraction coefficients a_1 and a_2:

$$\begin{aligned} \partial_t R &= \alpha R - \beta I - a_1\, \partial_x^2 I \\ \partial_t I &= \gamma R - \delta I + a_2\, \partial_x^2 R \end{aligned} \tag{3.6}$$

Following the method described in Ref. [4], the linear stability analysis of the homogenous state gives:

$$\begin{aligned} &\lambda^2 + \lambda(\delta - \alpha) + h(k^2) = 0 \\ &h(k^2) = a_1 a_2 k^4 - k^2(a_1\gamma + a_2\beta) + \gamma\beta - \delta\alpha \end{aligned} \tag{3.7}$$

where λ are the stability eigenvalues. It is easy to find that the wave-vector k corresponding to the minimum stability value is

$$k_c^2 = \left(\frac{2\pi}{\Lambda}\right)^2 = \frac{1}{2}\left[\frac{\beta}{a_1} + \frac{\gamma}{a_2}\right]. \tag{3.8}$$

Pattern formation is certainly inhibited when both a_1 and a_2 are negative. The presence of a region in the (a_1, a_2) plane where pattern formation is forbidden satisfies condition (b) of the Turing instability as described in Sect. 2. In the specific case of the DOPO, $a = a_1 = a_2$ and $\beta = \gamma = -\Delta$, resulting in $k_c^2 = -\Delta/a$ which is the typical condition of 'off-resonance' pattern formation (we recall that Δ is the cavity-medium detuning). We can then conclude that the so-called 'off-resonance' mechanism leading to pattern formation in DOPO and saturable absorbers *is a Turing instability* and that the stationary and spatially periodic structures observed in these photonic systems *are Turing patterns*. We note that an attempt to explain the relationship between optical and Turing patterns in OPO was discussed in Ref. [13]. We have extended the analogy (equivalence) to a single complex equation such as the PFGL model.

Important experiments on spatial structures in photonics originated in the late 1980s with the pioneering work of Giusfredi et al. [14] using a curved feedback mirror and Grynberg et al. [15] using pulsed counter-propagating beams, both in sodium vapours. Since then, clear-cut hexagonal patterns breaking the translational invariance have been observed in a multiplicity of photonic experiments using alkali atom [16,17], photorefractive [18] and liquid crystal [19,20] media. Many of these experiments have been based on the so-called "single-feedback-mirror" configuration originally studied theoretically by Firth and D'Alessandro at Strathclyde [21]. Such a set-up is presented schematically in Fig. 3. A laser beam passes through a nonlinear medium

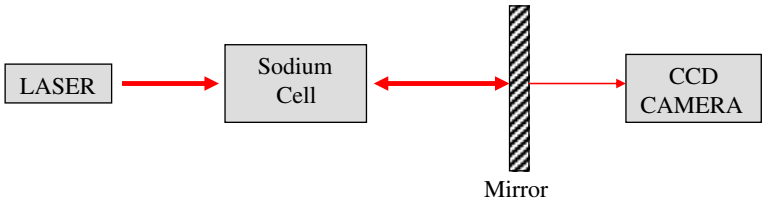

Fig. 3 Single mirror feedback configuration used for the formation of photonic patterns in [16,22]

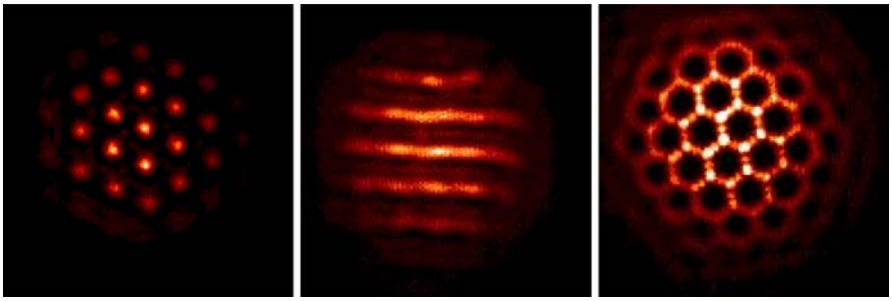

Fig. 4 Spatially periodic stationary structures in photonics: hexagons, rolls and honeycombs. The experiment comprises of a sodium cell and a single mirror feedback (see Ref. [16,22]). Courtesy of T. Ackemann

and is reflected by a single mirror back into the cell. Diffraction takes place mainly during free propagation from the cell to the mirror and back [21].

By using a single-mirror-feedback configuration with sodium vapours hexagonal, stripe and honeycomb structures (see Fig. 4) have been observed experimentally. The absence of a cavity makes the analysis far too complicated to establish an equivalence of these structures to Turing patterns. For this reason we label them 'photonic patterns'. Figure 4 clearly shows that when dealing with stationary patterns, photonics offers the possibility of performing '*dry-hydrodynamics*' or '*non-smelling chemistry*'.

4 Negative feedback control of Turing patterns

It was James Clerk Maxwell, the genius of Scottish mathematical physics, who established the theory of control systems on a firm basis of differential equations in his seminal paper *"On governors"* in 1868 [23]. Maxwell's work analysed the stability of James Watt's fly-ball governor that tried to control the speed of a steam engine. It also contained the embryonic idea of Negative Feedback Control (NFC) where part of a system's output is inverted and fed into the system's input to discourage certain unwanted features and produce a stable desired output. NFC led to the invention of the thermostat in 1885.

In 1996 at Strathclyde we developed a negative feedback scheme for the control of Turing patterns in photonics [24]. One important difference between photonics and chemistry is that the time scale for the formation of regular spatial structures varies from microseconds to several seconds. For practical applications, a control method

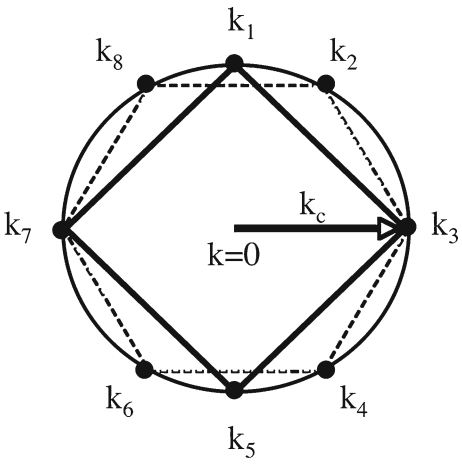

Fig. 5 Turing patterns in Fourier space. The spots are on the circle of radius k_c, the unstable wave-vector of the Turing instability. Different patterns have a different number and geometrical arrangement of spots. Patterns with different orientations are obtained by solid-body rotation of the spots around the centre $k=0$

in photonics has to be much faster than that in chemical experiments. For this reason we focused on feedback techniques that employed lenses, filters and optical elements to achieve control within photonic time scales. We will see towards the end of this section that the same methods can be applied to slower forming Turing structures such as those observed in chemical reactions, by using electronically calculated negative feedbacks.

An important obstacle in controlling Turing patterns is that they are spatially extended and, in principle, one would need 2D arrays of fast detectors to evaluate the appropriate feedback signal. Turing patterns have, however, a very compact representation in Fourier space. By making reference to Fig. 5, a stripe pattern of wavelength $\Lambda_c = 2\pi/k_c$ is transformed in Fourier space into two points, say k_1, k_5. Analogously, a square (hexagonal) pattern is transformed in Fourier space into four (six) points k_1, k_3, k_5, k_7 (k_2, k_3, k_4, k_6, k_7, k_8). All these Fourier representations can rotate as a solid body on a circle of radius k_c depending on the orientation of the pattern in space.

For completeness, we note that hexagons (H^+) and honeycombs (H^-) differ from each other in the condition imposed on their phases. These conditions are, respectively,

$$\begin{aligned} \phi_2 + \phi_4 + \phi_7 &= 2n\pi \\ \phi_2 + \phi_4 + \phi_7 &= (2n+1)\pi \end{aligned} \tag{4.1}$$

Finally, the homogeneous solution (that is unstable above the Turing instability) is a single spot at the centre of the Fourier space (corresponding to $k=0$). Note that finite size effects broaden the Fourier spots but do not change their position. The simultaneous existence of several stationary patterns of different geometries above a Turing instability (corresponding to separate fixed points in a global phase space) requires nonlinearity that, in turn, rules the pattern stability. It is the aim of this section to describe a control method that acts on the relative stability of the different patterns without however changing their shape and geometry.

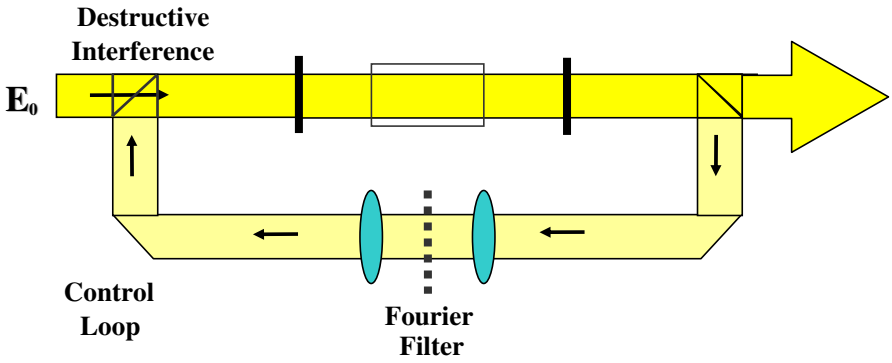

Fig. 6 The scheme for the NFC of Turing patterns in Fourier space

Fourier space is the optimal place where to implement control techniques to effectively operate on the stability of the Turing and photonic structures [3,24,25]. The idea behind our control method is to discourage spatial structures that are different from that of a target state through an appropriate negative feedback. The latter is achieved in the following way (see Fig. 6). A small part of the laser output is Fourier transformed, filtered in Fourier space by removing the Fourier components of the target state, inversely Fourier transformed and then added "negatively" to the input of the system.

For clarity, we make reference to the dynamical equation describing an optical absorber consisting of two-level atoms in a cavity with two transverse dimensions [26,27]:

$$\partial_t E = E_I - (1 + i\Delta)E - \frac{2C}{1 + |E|^2}E + ia\nabla^2 E, \tag{4.2}$$

where Δ is the cavity-medium detuning, C the coefficient of linear absorption of the medium and E_I the input pump field. We first show that (4.2) displays Turing patterns via an off-resonance mechanism and find the appropriate threshold. By introducing the normalized field A through $E = E_S(1+A)$, where E_S is the stationary homogeneous solution of (4.2), Eq. 4.2 becomes:

$$\partial_t A = \frac{2C}{1 + I} - (1 + i\Delta)A - \frac{2C(1 + A)}{1 + I(1 + A)(1 + A^*)} + ia\nabla^2 A, \tag{4.3}$$

where $I = E_S^2$. In the limit of $|A| << 1$, (4.3) is linearized to:

$$\partial_t A = (BI)A^* - (1 + B + i\Delta)A + ia\nabla^2 A, \tag{4.4}$$

where $B = 2C/(1+I)^2$. Separating the field A into its real and imaginary parts $A = R+iJ$ we obtain:

$$\partial_t R = [B(I-1)-1]R + \Delta J - a\,\nabla^2 J$$
$$\partial_t J = -\Delta R - [1+B(1+I)]J + a\,\nabla^2 R. \tag{4.5}$$

These equations are nothing else than those of the activator-inhibitor model seen in the section 3 and reveal that the homogeneous steady state undergoes a Turing instability for

$$2C > \frac{(1+I)^2}{I-1}, \tag{4.6}$$

leading to patterns at a critical wave-vector $k_c^2 = -\Delta/a$. We note that a more sophisticated nonlinear analysis shows that the imaginary part J is slaved to the real part R so that the latter first grows linearly like (4.5) and then saturates the pattern via suitable nonlinear terms [27]. The relative stability of different Turing patterns is ruled by the nonlinear terms that have been neglected in deriving Eq. 4.4.

Figure 6 is the optical implementation of the control technique for the saturable absorber case [24]. One advantage of photonics with respect to chemistry and/or hydrodynamics is that the direct and inverse Fourier transforms can be implemented experimentally by the simple use of lenses. The control signal is given by

$$f(x,y) = F^{-1}UF\,\mu E, \tag{4.7}$$

where F (F^{-1}) is the direct (inverse) Fourier transform, U is the filtering operation, and μ is a real parameter smaller than 1 and describing the magnitude of the control signal with respect to the output field E of Eq. 4.2. The control signal is then added "negatively" (optically through destructive interference) to the input field in Eq. 4.2, i.e.

$$E_I(x,y) = E_{0I}[1 - f(x,y)]. \tag{4.8}$$

Thus, the control increases the losses (dissipations) of every spatial component that is not contained in the target structure. In these terms, the control of Turing patterns with Fourier filtering is a real NFC technique. We also note that once the target pattern is attained, the feedback signal vanishes since the Fourier filter removes it entirely. This means that the controlled structure is a true solution of the system without feedback [24]. If such solution is unstable to other patterns, perturbations are expected to grow but their action is cancelled by the feedback signal and the system is pushed back to the 'unstable' state. This point was clarified in Ref. [28] where techniques based on the injection of stationary patterns are shown to be modification of unstable states instead of control methods.

Figure 7 shows the sum of the amplitudes of the modes on the critical wave-vector circle (see Fig. 5) versus the parameter $I = |E_S|^2$ for C=4.4 and control feedback strength $\mu = 0.05$ [24]. Control of several Turing patterns as well as the homogeneous solution by Fourier feedback is achieved in the saturable absorber system described by Eq. 4.2. In Fig. 7 the dashed (solid) lines correspond to controlled unstable (stable) stationary solutions. Since multi-stability is commonplace in systems forming Turing

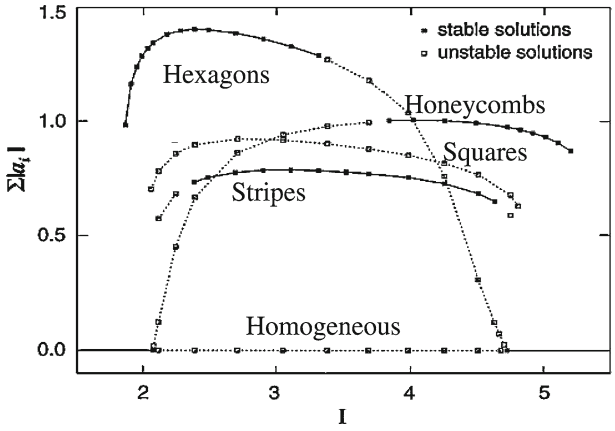

Fig. 7 Mode amplitudes of the pattern solutions versus the intensity of the stationary homogeneous state I [24]. Solid (dashed) lines correspond to stable (unstable) solutions of Eq. 4.2

patterns, control of stable states means that our technique is capable of reaching the (stable) target state starting from a different stable solution.

In the case of the control (stabilization) of homogeneous states, the Fourier filter is simply a small dark disk centered on the optical axis. All components corresponding to spatially changing structures are now subjected to increased losses due to the feedback control signal. The Turing instability is then completely suppressed (see horizontal line in Fig. 7) [24].

Turing patterns with given geometries are now available for the operator's choice [3]. A stripe, square and hexagonal filter can select, control and track the desired geometries. The idea of suppressing instabilities seen for the homogeneous case can now be extended to the patterned solutions when in the presence of spatio-temporal disorder. Application of the Fourier NFC methods to suppress turbulent behavior in photonic systems has been suggested and theoretically demonstrated in [25].

Photonic experiments : The Fourier negative feedback method to control photonic patterns has been successfully applied to a plethora of experimental realizations since the late 1990s [3]. These range from photorefractive [29], liquid crystal [30–32] and single-mirror vapour cells [33] systems. In particular in [31] both the control of photonic patterns (see Fig. 8) and the elimination of spatio-temporal turbulence have been achieved with the technique explained above.

Relevance to chemistry : Control of spatio-temporal structures in chemistry has been an important topic of research for some years (see the review article [34] and references therein). Because of the importance and relevance of waves, fronts and spirals, control of spatio-temporal structures in chemistry has focused on oscillatory and excitable systems more than on stationary Turing structures [34]. For example, unstable waves have been stabilized in a photosensitive BZ reaction by a negative feedback signal obtained by imaging the concentration of a reagent and using local and averaged light intensities of the image [35]. Fourier components have been used in chemistry

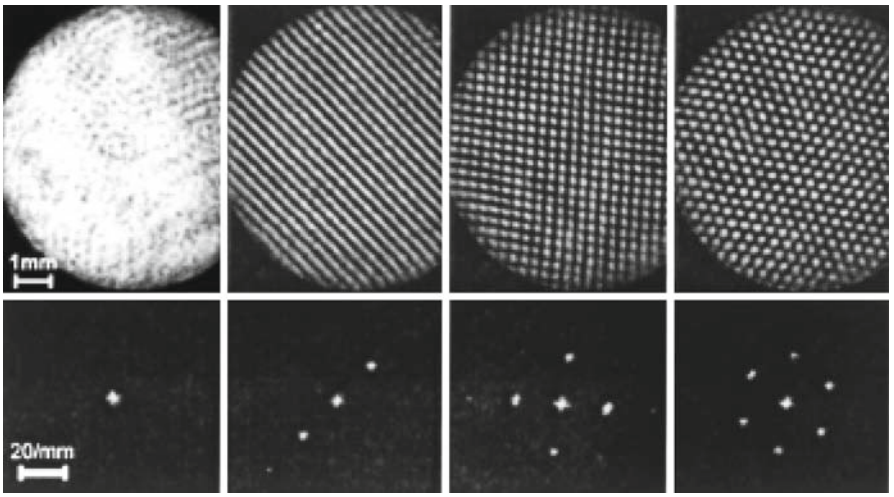

Fig. 8 Experimental control of photonic patterns [31]. Stabilized output structures (homogeneous, stripes, squares and hexagons) (top) and their Fourier transforms (bottom). Courtesy of E. Benkler

to control spatial structures in oxidation of CO on Pt(1 1 0) by using images of the concentrations and the modulation of the CO partial pressure in the reactor [36]. The Fourier transforms used in the evaluation of the control signal have been performed on computers via Fast Fourier Transform (FFT) algorithms [36].

The time scales in chemical experiments on stationary Turing patterns are far slower that those of photonics [5,6,9]. This simple fact removes the need for optical implementation of the Fourier transform. Implementation of the Fourier NFC method developed in Refs. [24,25] to chemical experiments displaying stationary Turing patterns, such as the CIMA [5,6] and the BZ-AOT [9], can be broken into these four steps:

(1) electronic detection of the optical images of the concentrations,
(2) computer evaluation of the Fourier transform of the optical image via FFT methods,
(3) filtering of the target structure and inverse Fourier transform on a computer,
(4) application of the obtained signal to control parameters of the reaction (such as reagent pressures, temperature, illumination for photosensitive cases, etc.) as a negative feedback.

5 Phase fronts, locked lines and locked spots

The previous sections clearly showed that several features and control methods of Turing structures are shared between photonic and chemical systems although the spatial coupling mechanisms, i.e. diffraction and diffusion, are intrinsically different. In this last section, we present a 'diffractive' effect on phase fronts that leads to localized spots that may have interest and possible extension in chemical systems.

Stationary and moving fronts separating two different phases have been at the centre of research in spatio-temporal structures in nonequilibrium systems for a long time

[37,38]. In systems with nonconserved order parameters (such as chemical concentrations), phase separation coarsens with a $t^{1/2}$ power law [39] and has been studied via Monte-Carlo simulations [37], coupled map systems [40], and integration of partial differential equations [12,38]. One difficulty in the experimental observation of the phase separation, and common to many branches of physics, is to maintain full equivalence (in energetic terms) of the two phases in order to avoid nucleation phenomena. In photonics, the DOPO offers the possibility of two perfectly equivalent states due to twin-photon generation in parametric down conversion (the opposite of second harmonic generation). In a DOPO, a pump field at frequency ω_0 gives rise in an optical cavity to a signal at frequency $\omega_1 = \omega_0/2$ by down-conversion. The dynamical equations are [11,12]:

$$\begin{aligned} \partial_t A_0 &= \Gamma(-A_0 + Q - A_1^2) + ia\nabla^2 A_0 \\ \partial_t A_1 &= -(1 + i\Delta)A_1 + A_0 A_1^* + 2ia\nabla^2 A_1 \end{aligned} \tag{5.1}$$

where A_0 and A_1 are the pump and signal fields, Γ is the ratio between the photon decay rates (i.e. mirror losses) at the two frequencies ω_0 and ω_1, $Q > 0$ is the (real) amplitude of the input pump, Δ is the signal detuning and a is the diffraction coefficient. In the case of no optical cavity for the pump field (Γ diverging to infinity), Eq. 5.1 reduce to:

$$\begin{aligned} A_0 &= Q - A_1^2 \\ \partial_t A_1 &= QA_1^* - (1 + i\Delta)A_1 - A_1|A_1|^2 + 2ia\nabla^2 A_1 \end{aligned} \tag{5.2}$$

The second equation in (5.2) is nothing else than the PFGL equation (3.4) discussed in Sect. 3 as a prototype for the formation of Turing structures for $\Delta < 0$. It is interesting to note that the more general form of the PFGL equation with complex parameters in front of every term [41], has played an important role in the description of resonantly forced reaction–diffusion systems in chemistry [34,41–43] such as the light sensitive BZ reaction [44]. Here we study the effect of the parameter Γ on the dynamics of phase fronts in the resonant case of $\Delta = 0$ [12].

For $\Delta = 0$ Eqs. 5.1 and 5.2 admit three homogenous solutions:

$$\begin{aligned} A_{0,s} &= Q - A_{1,s}^2 \\ A_{1,s} &= 0, \quad \pm\sqrt{Q-1} \end{aligned} \tag{5.3}$$

with the zero solution being stable for $Q < 1$ and unstable otherwise, and the two-phase solution existing and being stable for $Q > 1$. The two-phase solutions are mirror images of each other, differ by a phase π and have the same intensity $|A_{1,s}|^2$. In one transverse dimension ($\nabla^2 \to \partial_x^2$), the PFGL equation (5.2) admits also the Ising (domain) wall solution

$$A_{1,w} = \pm\sqrt{Q-1}\ \tanh\left[\sqrt{\frac{Q-1}{2}}\ x\right], \tag{5.4}$$

that connects the two homogeneous phase solutions. For generic Γ, Eq. 5.1 are non-variational and an explicit form of the Ising wall solution is not available (see also below). Accurate numerical methods for the determination of stationary (and travelling) spatial solutions have found the existence and stability of Ising walls (of more complicated form than a simple hyperbolic tangent) for a wide range of Γ values and Q>1 in Eq. 5.1 [12]. Ising domain walls in DOPO pass through zero and are symmetric with respect to the (now unstable) zero solution. There is then a point of zero intensity in the signal field in the middle of each Ising domain wall. When the pump field is resonated (see Eq. 5.1), the field A_0 not only presents a maximum where the signal field is zero (see the first equation of (5.3)) but it also 'diffracts' through this small aperture and develops oscillatory tails typical of Airy functions. These 'diffractive' oscillatory tails of the pump field affect, in turn, the shape of the Ising domain wall (5.4) and the signal field develops oscillatory tails close to the homogeneous phases. In the first panel of Fig. 9 oscillatory tails of two (interacting) Ising domain walls are clearly visible. The presence of these oscillatory tails is a nontrivial spatial feature since they are capable of stabilizing an entire family of localized states [12,45]. The interaction force between two Ising walls with oscillatory tails is spatially modulated with attractive (repulsive) locations where its minima (maxima) are located [45]. The depth (height) of these minima (maxima) increases the shorter the distance between the Ising domain walls. Figure 9 shows six of these locked localized states for the DOPO system (5.1) with $\Gamma = 1$ and Q=2 [12]. All these solutions are stationary, stable and coexist with their counterpart obtained by reflection around the horizontal x-axis (top-bottom exchange).

The solutions of Fig. 9 correspond to locked and parallel domain walls in two transverse dimensions. In 2D it is natural to consider the behaviour of one phase surrounded by the other and the phenomenon of phase separation. Figure 10 shows the long-term evolution of the signal intensity $|A_1|^2$ in simulations of Eq. 5.1 for $\Gamma = 1$ and Q=1.4 (left panel) and Q=2.5 (right panel). The black lines are the core of Ising walls where the signal intensity is zero.

We have verified that the dynamics of the phase domains follows the Allen-Cahn coarsening when the asymptotic state of the dynamics is exactly one or the other of the two phases (see the left panel of Fig. 10) by evaluating the structure factor S(K,t) where K is the transverse wave-vector, i.e. the Fourier transform of the two-point correlation function. The logarithm of $S(K,t)/t^{1/2}$ is plotted in Fig. 11 versus $kt^{1/2}$ at time intervals of 30 from t=30 to 300. Clearly the dynamics of the phase domains of (5.1) and (5.2) is ruled by local curvature effects with a $t^{1/2}$ growth-law [12].

The long-term dynamics and final state are modified when the input pump amplitude Q is increased. Above the critical value of Q=2.21, locked domain walls of circular shape appear (see the right panel of Fig. 10). Domains of one phase embedded in the other no longer shrink to zero but collapse onto circular spots whose stability is due to the self-locking of the inner oscillatory tail of the domain wall. These circular stable spots, discovered in Ref. [46] and also known as 'Dark Ring Cavity Solitons',

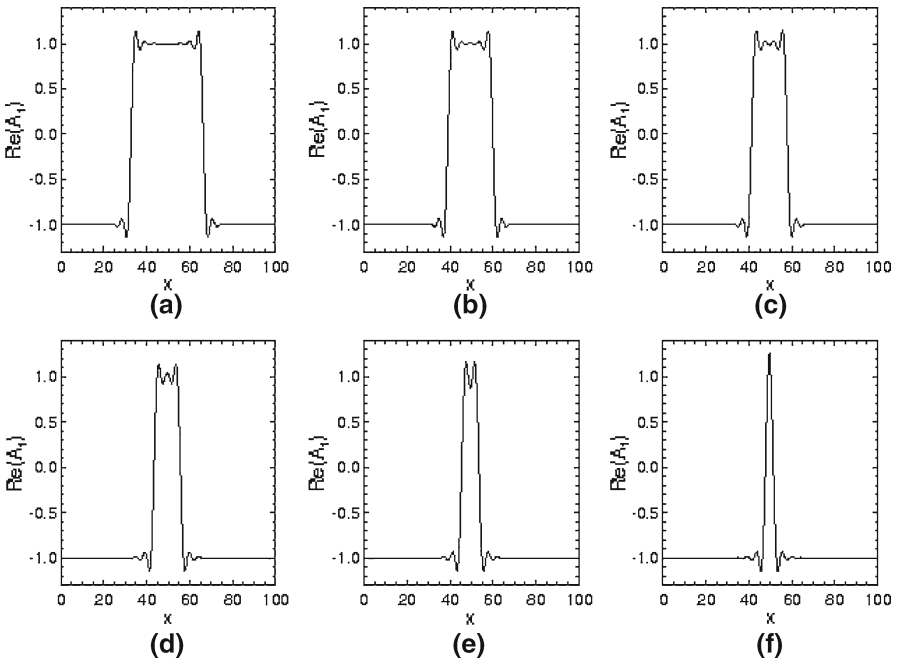

Fig. 9 Stable locked Ising walls in DOPO (5.1) in one transverse dimension for $\Gamma = 1$ and Q=2 [12]

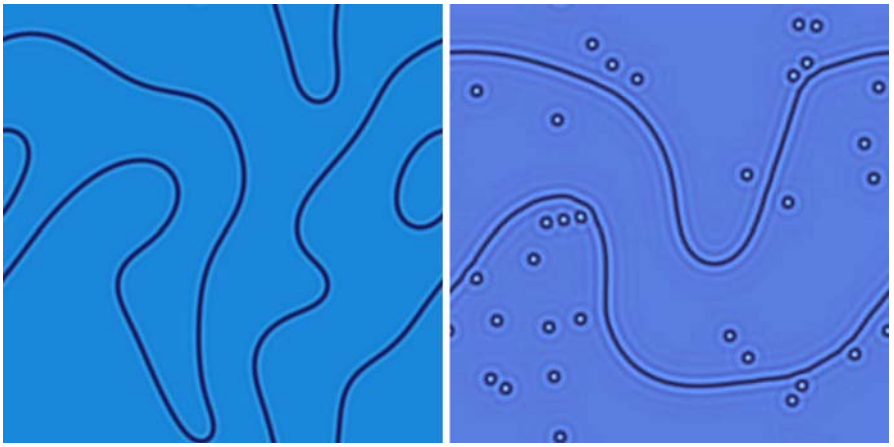

Fig. 10 Snapshots of the time evolution of the signal intensity $|A_1^2$ at t=1500 from Eq. 5.1 with $\Gamma = 1$, Q=1.4 (left panel) and Q=2.5 (right panel)

are the 2D counterpart of the localized locked Ising walls described in the 1D system. The dark ring of these structures is what remains of the circular Ising domain wall separating the two phases. Since localized states with circular symmetry have a zero eigenvalue (marginal stability) for translational motion [47], it is possible to move and pin these structures to maxima and minima of appropriate spatial modulations

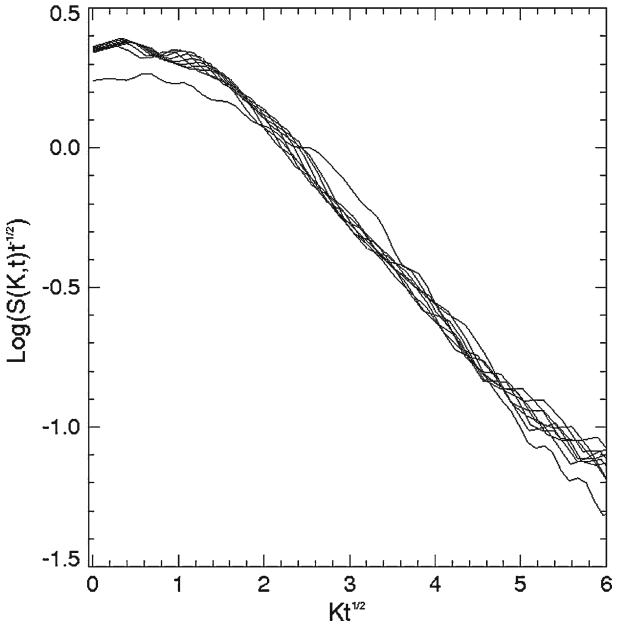

Fig. 11 The logarithm of the normalized structure factor versus $kt^{1/2}$ at time intervals of 30 from t = 30 to t = 300 from Eq. 5.1 with $\Gamma = 1$ and Q = 1.4 [12]. This figure is 'totally' dedicated to Ray Kapral

of the input pump beam [48]. Arrays of circular locked spots can thus be arranged and manipulated by the operator at will by using background modulations [48]. This procedure represents a first step in the '*control*' of fronts separating two phases.

Recent experiments performed with a cell of optically pumped sodium vapour in front of a single feedback mirror as described in Sect. 3 have used polarization domains as equivalent but separate phases [49]. The Allen-Cahn $t^{1/2}$-growth law and circular locked spots have been experimentally verified [49] in close agreement with the theory and simulations described here.

Complex dynamics of the PFGL equation have been used to describe reaction–diffusion systems in chemistry with several interacting species [41–43]. The addition or inclusion of a further component can, in principle, have the 'diffractive' effect that leads to oscillatory tails of the phase fronts in resonantly forced chemical reactions. We then expect the locking phenomena of fronts that occur in photonics to extend to chemical and biological systems. Again, diffraction and diffusion intertwine as their common mathematical description through the Laplacian operator has long suggested.

6 Conclusions

Photonics and chemistry are separate fields of scientific investigation and yet share a great deal of common features when it comes to spatio-temporal structures in the presence of nonlinearity. We hope to have demonstrated that the universality of Turing

patterns and phase fronts dynamics extends across these two disciplines in a deeper way than previously thought.

Control of Turing structures via Fourier methods and locked phase fronts are just two of the photonic features that can be extended to chemical systems. Diffractive effects in multi-component reaction–diffusion systems as well as diffusive effects in multi-field photonic devices allow for a fruitful exchange of scientific ideas across the separation of the research fields. In particular the study of universal models such as the periodically forced complex Ginzburg-Landau and the Swift-Hohenberg equations can provide useful insights for both disciplines.

Acknowledgements I would like to take advantage of this occasion to thank Ray Kapral for his constant support, kindness, teaching and patience during the last 22 years and for making my stage at the University of Toronto a memorable experience. Thanks to H.L Swinney, T. Ackemann and E. Benkler for providing Figs. 2, 4 and 8. Special thanks to A.M. Yao and T. Ackemann for a critical reading of the manuscript. Thanks also to W.J. Firth, A.J. Scroggie, R. Martin, D. Gomila, A.M. Yao, J. Jeffers, T. Ackemann, F. Papoff, G. Harkness, G. D'Alessandro, R. Neubecker, E. Benkler, W. Lange, C. Denz, P. Colet, M. San Miguel, L. Lugiato and to all the researchers who have collaborated with me in the work presented here. Financial support from the EU network FunFACS is gratefully acknowledged. I do apologize for not having studied enough fundamental chemistry at university; any error in the presentation of the material related to chemistry is my responsibility.

References

1. A.M. Turing, Philos. Trans. R. Soc. London B **237**, 37 (1952)
2. M.C. Cross, P.C. Hohenberg, Rev. Mod. Phys. **65**, 851 (1993)
3. G.K. Harkness, G.-L. Oppo, W.J. Firth, *Optics and Photonics News* (1998), p. 44
4. J.D. Murray, *Mathematical Biology* (Springer, Berlin, 1989)
5. V. Castets, E. Dulos, J. Boissonade, P. de Kepper, Phys. Rev. Lett. **64**, 2953 (1990); P. de Kepper, V. Castets, E. Dulos, J. Boissonade, Physica D **49**, 161 (1991); J. Boissonade, E. Dulos, P. de Kepper, in *Chemical Waves and Patterns* ed. by R. Kapral, K. Showalter (Kluwer, Dordrecht, 1995) p. 221
6. Q. Ouyang, H.L. Swinney, Nature **352**, 610 (1991); Q. Ouyang, H.L. Swinney, in *Chemical Waves and Patterns* ed. by R. Kapral, K. Showalter (Kluwer, Dordrecht, 1995) p. 269
7. S.C. Muller, J. Ross, J. Phys. Chem. A**107**, 7997 (2003)
8. M. Flicker, J. Ross, J. Phys. Chem. **60**, 3458 (1973)
9. V.K. Vanag, I. Epstein, Phys. Rev. Lett. **87**, 228301 (2001)
10. L.A. Lugiato, R. Lefever, Phys. Rev. Lett. **58**, 2209 (1987)
11. G.-L. Oppo, M. Brambilla, L.A. Lugiato, Phys. Rev. A **49**, 2028 (1994)
12. G.-L. Oppo, A.J. Scroggie and W.J. Firth, Phys. Rev. E **63**, 066209 (2001)
13. K. Staliunas, V.J. Sanchez-Morcillo, Opt. Comm. **177**, 389 (2000)
14. G. Giusfredi et al., J. Opt. Soc. Am. B **5**, 1181 (1988)
15. G. Grynberg, E. Le Bihan, P. Verkerk, P. Simoneau, J.R. Leite, D. Bloch, S. Le Boiteux, M. Ducloy, Opt. Comm. **67**, 363 (1988)
16. A. Petrossian, M. Pinard, A. Maitre, J.Y. Courtois, G. Grynberg, Eur. Phys. Lett. **18**, 689 (1992)
17. T. Ackemann, W. Lange, Phys. Rev. A **50**, R4468 (1994)
18. T. Honda, Opt. Lett. **18**, 598 (1993); T. Honda, Opt. Lett. **20**, 851 (1995); T. Honda, H. Matsumoto, Opt. Lett. **20**, 1755 (1995); A.V. Mamaev, M. Saffman, Opt. Lett. **22**, 283 (1997); C. Denz, M. Schwab, M. Sedlatsheck, T. Tschudi, T. Honda, J. Opt. Soc. Am. B **15**, 2057 (1998)
19. R. McDonald, H.J. Eichler, Opt. Comm. **89**, 289 (1992); M. Tamburrini, M. Boanvita, S. Wabnitz, E. Santamato, Opt. Lett. **18**, 855 (1993)
20. B. Thuring, R. Neubecker, T. Tschudi, Opt. Comm. **102**, 111 (1993); E. Papmaploni, S. Residori, F.T. Arecchi, Opt. Lett. **24**, 647 (1993)
21. W.J. Firth, J. Mod. Opt. **37**, 151 (1990); G. D'Alessandro, W.J. Firth, Phys. Rev. Lett. **66**, 2597 (1991); G. D'Alessandro, W.J. Firth, Phys. Rev. A **46**, 537 (1992)

22. T. Ackemann, Y. Logvin, A. Heuer, W. Lange, Phys. Rev. Lett. **75**, 3450 (1995); W. Lange, Y. Logvin, T. Ackemann, Physica D **96**, 230 (1996); T. Ackemann, W. Lange, App. Phys. B **72**, 21 (2001)
23. J.C. Maxwell, Proc. R. Soc. London **16**, 279 (1868)
24. R. Martin, A.J. Scroggie, G.-L. Oppo, W.J. Firth, Phys. Rev. Lett. **77**, 4007 (1996)
25. G.K. Harkness, G.-L. Oppo, R. Martin, A.J. Scroggie, W.J. Firth, Phys. Rev. A **58**, 2577 (1998)
26. L.A. Lugiato, C. Oldano, Phys. Rev. A **37**, 3896 (1988)
27. W.J. Firth, A.J. Scroggie, Europhys. Lett. **26**, 521 (1994)
28. G.K. Harkness, R. Martin, G.-L. Oppo, A.J. Scroggie, W.J. Firth, Phys. Rev. Lett. **82**, 2406 (1999)
29. A.V. Mamaev, M. Saffman, Phys. Rev. Lett. **80**, 3499 (1998); S.J. Jensen, M. Schwab, C. Denz, Phys. Rev. Lett. **81**, 1614 (1998); Y. Hayasaki, H. Yamamoto, N. Nishida, Opt. Comm. **187**, 49 (2001)
30. G.K. Harkness, G.-L. Oppo, E. Benkler, M. Kreuzer, R. Neubecker, T. Tschudi, J. Opt. B **1**, 177 (1999)
31. E. Benkler, M. Kreuzer, R. Neubecker, T. Tschudi, Phys. Rev. Lett. **84**, 879 (2000)
32. R. Neubecker, E. Benkler, Phys. Rev. E **65**, 066206 (2002); R. Neubecker, E. Benkler, R. Martin, G.-L. Oppo, Phys. Rev. Lett. **91**, 113903 (2003)
33. T. Ackemann, B. Giese, B. Shapers, W. Lange, J. Opt. B **1**, 70 (1999); R. Herrero, E. Große Westhoff, A. Aumann, T. Ackemann, Y. Logvin, W. Lange, Phys. Rev. Lett. **82**, 4627 (1999)
34. A.S. Mikhailov, K. Showalter, Phys. Rep. **425**, 79 (2006)
35. E. Mihaliuk, T. Sakurai, F. Chirila, K. Showalter, Phys. Rev. E **65**, 0656021 (2002); V. Zykov, K. Showalter, Phys. Rev. Lett. **94**, 0683021 (2005)
36. H.H. Rotermund, J. Electron. Spectrosc. Relat. Phenom. **99**, 41 (1999); C. Beta, M.G. Moula, A.S. Mikhailov, H.H. Rotermund, G. Ertl, Phys. Rev. Lett. **93**, 1883021 (2004)
37. J.D. Gunton, M. San Miguel, P. Sahni, in *Phase Transitions and Critical Phenomena*, ed. by C. Domb, J. Lebowitz (Academic Press, New York, 1983)
38. A. Bray, Adv. Phys. **43**, 357 (1994)
39. S.M. Allen, J.W. Cahn, Acta Metall. **27**, 1085 (1979)
40. R. Kapral, G.-L. Oppo, Physica D **23**, 455 (1986); G.-L. Oppo, R. Kapral, Phys. Rev. A **36**, 5820 (1987)
41. It may seem strange that 'diffraction-like' terms appear in the description of reaction–diffusion systems. For a derivation of the complex Ginzburg-Landau equation from the Brusselator model see Y. Kuramoto, *Chemical Oscillations, Waves and Turbulence* (Springer, New York, 1984)
42. C. Hemming, R. Kapral, Physca A **306**, 199 (2002)
43. O. Rudzick, A.S. Mikhailov, Phys. Rev. Lett. **96**, 018302 (2006)
44. V. Petrov, Q. Ouyang, H.L. Swinney, Nature **388**, 655 (1997); A.L. Lin, A. Hagberg, A. Ardelea, M. Bertram, H.L. Swinney, E. Meron, Phys. Rev. E **62**, 3790 (2000)
45. P. Coullet, C. Elphick, D. Repaux, Phys. Rev. Lett. **58**, 431 (1987); P. Coullet, Int. J. Bif. Chaos **12**, 2445 (2002)
46. G.-L. Oppo, A.J. Scroggie, W.J. Firth, J. Opt. B **1**, 133 (1999)
47. W.J. Firth, A.J. Scroggie, Phys. Rev. Lett. **76**, 1623 (1996)
48. A.J. Scroggie, J. Jeffers, G. McCartney, G.-L. Oppo, Phys. Rev. E **71**, 046602 (2005)
49. M. Pesch, W. Lange, D. Gomila, T. Ackemann, W.J. Firth, G.-L. Oppo, Phys. Rev. Lett. **99**, 153902 (2007)